Online Monitoring of Aluminum Electrolytic Capacitors in Photovoltaic Systems by Magnetoresistive Sensors

Wenchao Miao, K. H. Lam, and Philip W. T. Pong, *Senior Member, IEEE*

***Abstract*—Due to the environmental concerns and new energy policies, worldwide expectations for energy production utilizing photovoltaic (PV) systems are increasing significantly. The aluminum electrolytic capacitor (AEC) is extensively used in filtering application for power electronic converters in PV systems since they can achieve the highest energy density with the lowest cost. However, the lifetime of an AEC is limited due to the electrolyte vaporization. The degradation of AECs challenges the efficiency and reliability of a PV system. Therefore, the health-monitoring of AECs is indispensable for the PV systems to operate reliably. In this paper, an online AEC-monitoring scheme based on magnetic-field sensing is proposed for PV systems under various working conditions. The AEC-monitoring technique using the equivalent series resistance (ESR) and capacitance (C) as the health indicators were developed for the power electronic converters in PV systems. The proposed methodology considering the voltage drops on C can improve the accuracy in ESR-estimation and achieve the estimation of C. The simulation results with Simulink verified that the proposed method was capable of estimating the health indicators accurately over various levels of solar irradiance and ambient temperature. The tunneling magnetoresistive (TMR) sensors were pre-calibrated from -25 to 100° C for implementation in PV systems. The experimental results proved that TMR sensors could measure the current of AECs effectively to achieve the precise estimations of the health indicators using the proposed technique. This technique is non-invasive, compact, and cost-effective since it can be realized with the TMR sensors or other MR sensors.**

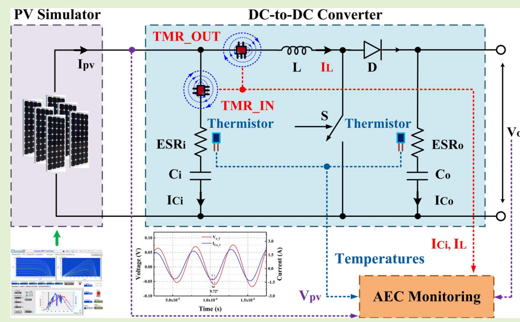

***Index Terms*—Aluminum electrolytic capacitor, condition monitoring, PV system, tunneling magnetoresistive sensor.**

I. Introduction

PHOTOVOLTAIC (PV) systems are one of the most popular renewable energy systems, and the installation of PV systems has been growing rapidly. According to the International Renewable Energy Agency (IRENA), the cumulative global PV installations reached 480 GW at the end of 2018 [1]. In the system level, there are ground faults, line-line faults, overcurrent faults and arc faults in a PV system [2]. The abnormal conditions of devices also hinder the normal operation of a PV system. In PV systems, the aluminum electrolytic capacitors (AECs) are widely used for filtering applications in power electronic converters due to their high energy density and low cost [3]–[5]. However, the electrolyte vaporization, which leads to a decrease in capacitance (C) and an increase in equivalent series resistance (ESR), restricts the lifetime of an AEC [3]. It is claimed that about 30 % of the failures in power electronic converters are caused by AECs [5], [6]. The AEC is one of the most vulnerable components in power electronic converters and challenges the reliability and efficiency of PV systems [7]–[9]. Therefore, the condition monitoring of AECs is essential to ensure the reliability and efficiency of PV systems.

It is a consensus that an AEC is worn out when its C reduces by 20%, or the ESR doubles its original value. Currently, the condition-monitoring techniques of AECs are mainly based on the estimations of their ESRs and Cs. The

Manuscript received September 17, 2019; accepted October 3, 2019. Date of publication October 7, 2019; date of current version December 31, 2019. This work was supported in part by the Seed Funding Program for Basic Research, in part by the Seed Funding Program for Applied Research, in part by the Small Project Funding Program from The University of Hong Kong, Hong Kong, in part by the Innovation and Technology Fund (ITF) Tier 3 Funding under Grant ITS/203/14, Grant ITS/104/13, and Grant ITS/214/14, in part by the Research Grants Council-General Research Fund (RGC-GRF) under Grant HKU 17204617, and in part by the University Grants Committee of Hong Kong under Contract AoE/P-04/08. The associate editor coordinating the review of this article and approving it for publication was Prof. Boby George. *(Corresponding author: Philip W. T. Pong.)*

The authors are with the Department of Electrical and Electronic Engineering, The University of Hong Kong, Hong Kong (e-mail: ppong@eee.hku.hk).

Digital Object Identifier 10.1109/JSEN.2019.2945943

condition-monitoring techniques can be classified as offline when an interruption of the system is required to acquire the health indicator or quasi-online when the health indicator is attained during the routine pause of the system or online when the health indicator can be obtained during the operation of the system [4], [10]. Although the offline [11]–[13] and quasi-online [14], [15] techniques adopting injected signals can achieve the estimations of ESRs and Cs, the reliability and efficiency of the systems are jeopardized by the interruptions. The online techniques utilizing the electrical circuits are able to monitor the AECs [16], [17], but the circuits need to be specially designed for applications in different systems and thus incurring extra costs. The specific equations to calculate the ESRs and Cs of AECs in power converters are derived in [18]–[21]. However, different methodologies are required for each topology of power converters. They cannot be applied in other power converters.

The online ripple method of using the voltage and current ripples of AECs can estimate the ESRs and Cs [22]–[28]. The voltage across the C of an AEC is neglected in the ripple method. However, there are cases that the voltage across the C is not negligible [12], [29]. As a result, the accuracy of this ripple method is not guaranteed. Albeit condition monitoring of AECs in PV systems also have been researched [4], [5], [8], [9], [30], the working conditions of PV systems vary with the levels of solar irradiance and ambient temperature. The ESRs and Cs of AECs are affected by the capacitor core temperature [24]. Hence, a comprehensive online AEC-monitoring technique for PV systems working in various conditions is desirable.

Furthermore, parasitic impedance (Z) is induced by the shunt resistor used for current measurement, which stresses the normal operation of power electronic converters [26]. The Hall-effect current transducers can attain the current ripples of AECs [4], [5], [8], [27], [30]. However, a magnetic concentrator concentrates the magnetic field of the target current is required by the current transducer, which largely increases the volume and expense of the device [31]. Besides, the bandwidth of the Hall sensor is limited, which is generally lower than 200 kHz [31]. Therefore, the Hall-effect current transducer of relatively large size, high cost, and narrow bandwidth is not applicable in measuring the high-frequency current in power electronic converters. Additionally, the performance of most current sensors is temperature dependent [31]. Hence, it is necessary to acquire the temperature effects on current sensors for implementations under various conditions in PV systems. In this way, the temperature effects on current sensors can be considered by using a thermistor to measure the temperature simultaneously.

In this paper, the voltage drops on C is considered in the proposed method to improve the accuracy of ESR-estimation and the equation to estimate C is derived. The tunneling magnetoresistive (TMR) sensor, which is competent for measuring the magnetic field [32]–[34], can be utilized to sense the current of AECs up to 1 MHz non-invasively. The low-cost TMR sensor is compact in size (typically less than 15 mm^3) and consume very little power (typically less than 0.4 mW), and it can be integrated on the printed circuit boards (PCBs) of power converters to measure the current effectively. The temperature effects on the TMR sensor was determined for implementations in PV systems. Thermistors were used to measure the temperatures of AECs for estimations of ESRs and Cs. A PV system was developed on Simulink to verify the proposed technique. The experimental results with the PV simulator confirmed that the proposed method could realize the online estimations of ESRs and Cs accurately under various working conditions. The proposed technique is also feasible for AEC-monitoring in other power electronic systems.

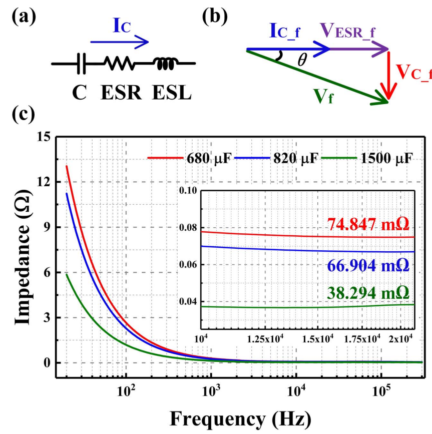

Fig. 1. The characteristics of AECs, (a) the equivalent circuit, (b) the phasor diagram of the voltage of an AEC, and (c) Zs of the AECs in 680, 820, and 1500 μF from 20 Hz to 300 kHz at 25 °C.

This paper is organized as follows. In Section II, the characteristics of AECs and principles of the AEC-monitoring technique are illustrated. The method to estimate the ESRs and Cs based on magnetic-field sensing are proposed. In Section III, the PV system is developed on Simulink to verify the proposed methodology in various conditions. In Section IV, the technique is verified by the experimental results with the PV simulator. The conclusion is drawn in Section V.

II. Principles of AEC and Online-Monitoring Methodology Based on Magnetic-Field Sensing

A. Characteristics and Condition-Monitoring Method of AEC

The simplified equivalent circuit of an AEC consists of C, ESR, and equivalent series inductance (ESL) as Fig. 1 (a) depicts. Therefore, the Z of an AEC can be expressed by Eq. (1).

$$\boldsymbol{Z = 1/j\omega C + ESR + j\omega ESL} \tag{1}$$

where ω is the frequency of current, I_c.

Hence, the voltage across the AEC can be calculated as

$$\boldsymbol{V = (1/j\omega C + ESR + j\omega ESL) \cdot I_C} \tag{2}$$

Therefore, the Z of an AEC can be attained by using the voltage and current ripples of the AEC. Since this ripple method is affected by the transient values of voltage and current ripples, the fundamental components of the voltage and current ripples should be used as expressed by Eq. (3).

$$\boldsymbol{Z = \Delta V_f / \Delta I_{C\_f}} \tag{3}$$

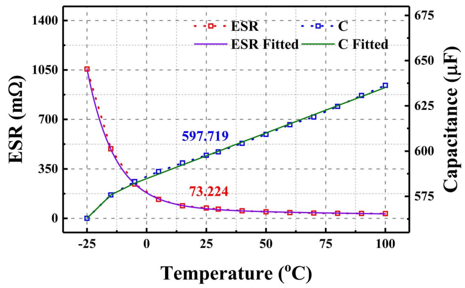

Fig. 2. The ESR at 20 kHz and capacitance at 120 Hz of the AEC in 680 μF from -25 to 100 °C.

The ESR is dominant in the Z and the voltage drops on ESL is negligible when the frequency is in tens to hundreds of kilohertz [26]. The operation frequency of a power electronic system is usually in this frequency range. Therefore, the ESRs of AECs in power electronic systems are calculated by using Eq. (3) in [22], [24], [25], and [27].

However, the voltage drops on C is contributing to the voltage ripple across the AEC apparently when the frequency is around several tens of kilohertz. The phasor diagram can be drawn as depicted in Fig. 1 (b). The current is leading the voltage by an angle of θ. In this case, the 1/jωC is relatively large and cannot be neglected. As shown in Fig. 1 (c), the Zs of the AECs from Nichicon in 680 and 820 μF, and Nippon Chemi-Con in 1500 μF decrease with the frequency as measured by the LCR meter (BK 891, BK Precision) at 25 °C. Although the Zs of the three AECs stay in almost constant values at the frequency around tens of kilohertz, their Zs still decrease slightly from 10 to 20 kHz to be 74.847, 66.904 and 38.294 mΩ at 20 kHz. This is due to the decreasing of 1/jωC. Therefore, the voltage drops on C is not negligible, and the ESR-estimation methodology needs to be further developed. To achieve a higher accuracy of the ESR-estimation [12], [29], the ESR should be calculated by using Eq. (4).

$$\boldsymbol{ESR = \Delta V_f Cos(\theta) / \Delta I_{C\_f}} \tag{4}$$

According to the phasor diagram, Eq. (5) can be deduced to estimate the Cs of AECs.

$$\boldsymbol{C = \Delta I_{C\_f} / (\Delta V_f Sin(\theta)\omega)} \tag{5}$$

Thus, the condition-monitoring of AECs can be achieved by estimating their ESRs and Cs by using Eq. (4) and (5).

However, the ESRs and Cs of AECs vary with the temperature. The thermal chamber (SH-242, ESPEC) was used to investigate the temperature effects on AECs. The ESR of the AEC of 680 μF decreases with the temperature from -25 to 100 °C as shown in Fig. 2. The ESR is 73.224 mΩ at 25 °C which is less than the Z of 74.847 mΩ. Hence, it verifies that it is essential to consider the voltage drops on C in the estimation of ESR. It is found that the ESR of an AEC decreases exponentially with the temperature [24], [35], and it can be expressed by Eq. (6).

$$\boldsymbol{ESR = \alpha + \beta \cdot e^{-T_C/\gamma}} \tag{6}$$

where α, β, and γ depend on the type of an AEC, T_c is the capacitor core temperature.

TABLE I
THE FITTING PARAMETERS OF EQ. (7)

C (μF)	α_1	β_1	γ_1	β_2	γ_2
680	-3.62	115.67	11.70	68.79	151.65
820	15.48	81.33	11.50	47.80	94.40
1500	22.49	26.21	11.282	17.89	45.89

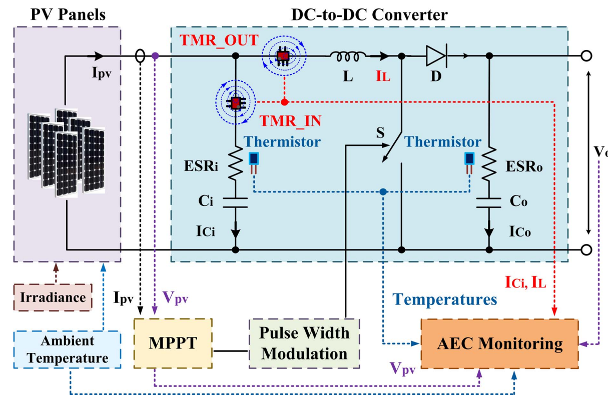

Fig. 3. The online condition-monitoring scheme of AECs in a PV system.

However, the ESR curves cannot be well fitted by Eq. (6) [24], [30]. The errors caused by Eq. (6) largely affect the accuracy of ESR estimation. To improve accuracy, Eq. (7) is derived.

$$\boldsymbol{ESR = \alpha_1 + \beta_1 \cdot e^{-T_C/\gamma_1} + \beta_2 \cdot e^{-T_C/\gamma_2}} \tag{7}$$

where α_1, β_1, β_2, γ_1, and γ_2 depend on the type of AEC.

The fitting results of the three AECs by using Eq. (7) are provided in Table I. Comparing to Eq. (6), the errors of the fitted ESRs can be reduced from around 17 % to be around 5 % by Eq. (7). The C of the AEC in 680 μF increases with the temperature, as shown in Fig. 2. It increases rapidly from -25 to 15 °C. Nevertheless, the growth rate decreases after 15 °C. Two linear equations are used to fit the capacitance at the temperature from -25 to 15 °C, and -15 to 100 °C separately as Fig. 2 depicts. The accuracy of using two separate linear equations for fitting the Cs of the three AECs is within 0.27%. Hence, the ESR and C of an AEC can be accurately modeled by Eq. (7) and linear equations so that the temperature effects on ESRs and Cs can be effectively considered in the AEC-monitoring.

B. Online-Monitoring Scheme of AECs

The online-monitoring scheme of AECs in PV systems can be developed as Fig. 3 depicts. The PV system consists of PV panels, a DC-to-DC converter, an maximum power point tracking (MPPT) controller, and the pulse width modulation (PWM) unit. A boost converter is used for the DC-to-DC conversion as an example in Fig. 3. The AECs are used in the boost converter for filtering the input and output voltages. The specifications of the boost converter at 25 °C are provided in Table II. The ESRs and Cs of AECs and L of the inductor are measured by the LCR meter. The AECs of 680 and 820 μF

TABLE II
SPECIFICATIONS OF THE BOOST CONVERTER AT 25 °C

Parameters	Symbol	Values
Input ESR at 20 kHz (mΩ)	ESR_i	73.224, 65.516
Input C at 120 Hz (μF)	C_i	597.719, 695.616
Output ESR at 20 kHz (mΩ)	ESR_o	36.775
Output C at 120 Hz (μF)	C_o	1331.414
Inductance (μH)	L	232.4
Switching Frequency (kHz)	f	20

are used as the input capacitor, and the AEC of 1500 μF is used as the output capacitor. According to the proposed approach, the voltage ripple of PV panels (ΔV_{pv}), the current ripple of input AEC (ΔI_{Ci}), the temperature of input AEC, the output voltage ripple (ΔV_o), the current ripple of output AEC (ΔI_{Co}), and the temperature of output AEC are required for the estimations of ESRs and Cs. In a boost converter, the ΔI_{Co} equals the peak of inductor current (I_L) [25], [28], therefore, the inductor current can be measured for the estimations of ESR and C of output AEC. In this way, the two sensors can be placed close to achieve the integration of the current-measurement circuit on the PCB as shown in Fig. 3.

The V_{pv} and V_o can be obtained from the PV system by voltage sensors, and they are also needed in MPPT and control purposes. Therefore, this method does not incur an extra cost. The temperatures of the AECs can be measured instantaneously by the thermistors [5], [17], [24], [26], [27]. The low-cost and non-invasive TMR sensors can be integrated on the PCB of the converter to measure the magnetic field of the I_{Ci} and I_L. The current is sensed by a TMR sensor based on the tunneling magnetoresistance effect of a magnetic tunnel junction (MTJ). The target current can be determined by the electrical resistance of the MTJ which changes as a function of the magnetic field emanated from the current [32]. Since the typical current consumption of a TMR2001 is 16 μA [34], which generates extremely low heat, the temperature of the TMR2001 during operation is almost the same as the ambient temperature. Therefore, the ambient temperature required in forecasting the performance of PV panels can be used to predict the temperature effects on TMR sensors [36]. Thus, a non-invasive, low-cost, and compact online AEC-monitoring system based on magnetic-field sensing can be developed for PV systems.

III. SIMULATIONS OF THE PV SYSTEM ON SIMULINK

The PV system was simulated on Simulink to investigate the proposed methodologies for estimations of ESRs and Cs of AECs. The proposed methodologies were verified with the PV system in different irradiance and temperature levels. It was also studied in transient conditions with the load varied from 100 to 50 Ω.

A. PV System on Simulink

The PV system was modeled on Simulink, as shown in Fig. 4. The PV array contains two parallel-connected strings

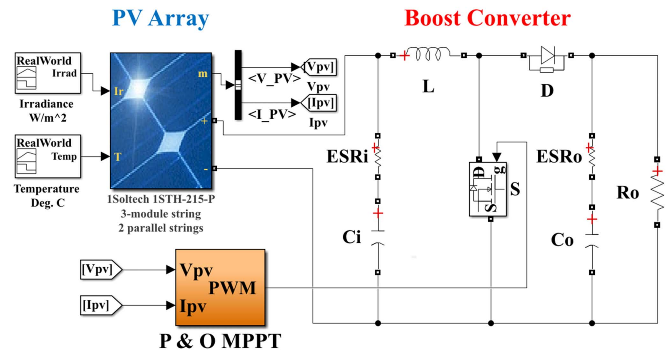

Fig. 4. The PV system on Simulink with the boost converter and the MPPT controller.

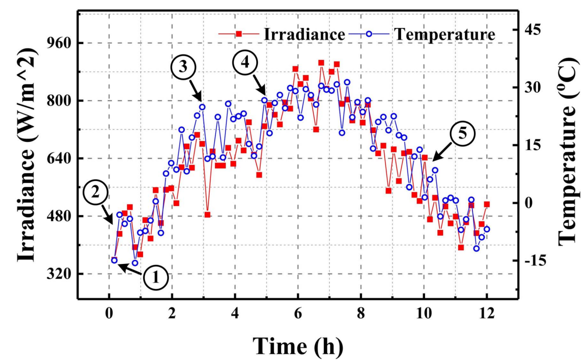

Fig. 5. The scaled irradiance and temperature levels in Urumqi of 12 hours.

with three series-connected PV panels (STH-215-P, Soltech) in each string. The levels of irradiance and temperature were imported to the PV array to simulate the generation of electrical energy. The specifications of the boost converter are provided in Table II. The AEC of 680 μF, which was 597.719 μF at 120 Hz with ESR of 73.224 mΩ at 20 kHz, was used as the input capacitor. The output capacitor was the AEC of 1500 μF, which was 1331.414 μF with ESR of 36.775 mΩ as provided in Table. II. The switching frequency of the boost converter was 20 kHz. The perturb and observe (P&O) method was used to develop the MPPT controller [37].

The irradiance and temperature levels of Urumqi (43.8°, 87.6°) vary widely in a year. Therefore, the irradiance and temperature data of Urumqi was used in the simulations to investigate the applicability of the proposed methodologies. The annual irradiance and temperature data of Urumqi were scaled to be in 12 hours, as shown in Fig. 5. The five cases of the irradiance and temperature levels were selected in Table III. The proposed methodologies were studied with the five cases of irradiance and temperature levels.

B. Simulation Results

The simulation results of case 1, when the irradiance and temperature levels were constant, are shown in Fig. 6. The voltage and current of the input AEC are V_{pv} and I_{Ci} as Fig. 6 (a) depicts. The digital bandpass filter on MATLAB, allowing frequencies between 19 and 21 kHz to pass, was used

TABLE III
THE IRRADIANCE AND TEMPERATURE LEVELS

Case	Irradiance (W/m^2)	Temperature (ºC)
1. Constant irradiance and temperature	359	-14.92
2. Irradiance and temperature increase	359 to 431	-14.92 to -3.06
3. Irradiance and temperature decrease	680 to 485	24.91 o 11.46
4. Irradiance increases and temperature decreases	729 to 788	26.67 o 18.11
5. Irradiance decreases and temperature increases	642 to 471	1.46 to 6.08

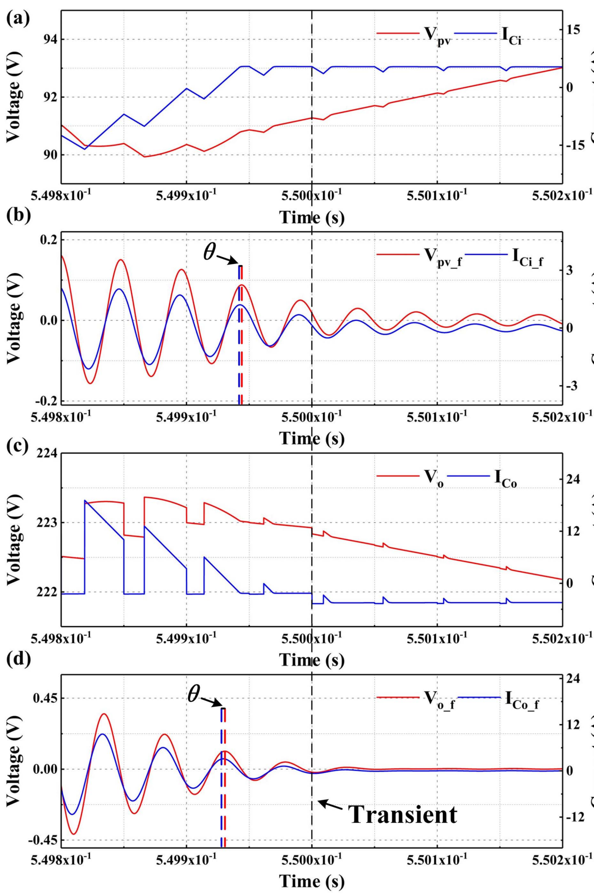

Fig. 6. Simulation results with the constant irradiance and temperature, (a) the voltage (V_{pv}) and current (I_{Ci}) of the input capacitor, and (b) their fundamental components, V_{pv_f} and I_{Ci_f}, (c) the voltage (V_o) and current (I_{Co}) of output capacitor, and (d) their fundamental components, V_{o_f} and I_{Co_f}.

to attain the fundamental components of the voltage and current. The fundamental components of V_{pv} and I_{Ci} are shown in Fig. 6 (b). Similarly, the voltage and current of the output AEC, and their fundamental components are shown in Fig. 6 (c) and (d), respectively. It can be seen that the current was leading the voltage by an angle of θ. The load varied from 100 to 50 Ω at 0.55 s leading to the transient of voltage and current, as shown in Fig 6.

TABLE IV
THE SIMULATION RESULTS OF THE INPUT CAPACITOR IN STEADY STATE

Case	θ (º)	Error of Eq. (3) (%)	Error of Eq. (4) (%)	Error of Eq. (5) (%)
1	10.15	1.19	-0.39	-0.63
2	10.61	1.72	-0.02	0.49
3	10.55	0.91	-0.79	0.80
4	10.55	2.69	0.95	0.69
5	10.13	1.67	0.09	-0.70

TABLE V
THE SIMULATION RESULTS OF THE INPUT CAPACITOR IN TRANSIENT

Case	θ (º)	Error of Eq. (3) (%)	Error of Eq. (4) (%)	Error of Eq. (5) (%)
1	10.27	1.41	-0.21	0.46
2	10.13	1.90	0.31	-0.91
3	10.55	1.18	-0.53	-1.14
4	10.35	0.84	-0.80	-0.58
5	10.73	2.10	0.32	-0.53

TABLE VI
THE SIMULATION RESULTS OF THE OUTPUT CAPACITOR IN STEADY STATE

Case	θ (º)	Error of Eq. (3) (%)	Error of Eq. (4) (%)	Error of Eq. (5) (%)
1	9.05	0.84	-0.41	-0.06
2	9.53	2.89	1.47	-0.85
3	9.05	0.88	-0.37	-0.10
4	9.05	0.87	0.38	-0.09
5	9.71	2.59	1.12	-0.68

TABLE VII
THE SIMULATION RESULTS OF THE OUTPUT CAPACITOR IN TRANSIENT

Case	θ (º)	Error of Eq. (3) (%)	Error of Eq. (4) (%)	Error of Eq. (5) (%)
1	9.30	1.35	0.02	-0.22
2	8.99	2.42	1.16	-0.39
3	9.19	1.43	0.13	0.24
4	8.82	2.67	1.46	1.22
5	9.05	0.70	-0.55	0.09

The simulation results of the AECs in the five cases at steady-state and transient conditions are presented in Table IV to VII. They verified that the errors of the estimated ESRs can be significantly reduced by the proposed method of using Eq. (4) to be within 1.48 %. The errors from Eq. (4) were less than half of the errors caused by Eq. (3) in both steady-state and transient conditions. It was also confirmed that Eq. (5) was capable of estimating the Cs of input and output AECs with an error of less than 1.23 %. In summary, the proposed approach can effectively improve the accuracy of ESR-estimation, and it can estimate the Cs of AECs accurately in PV systems over various irradiance and temperature levels.

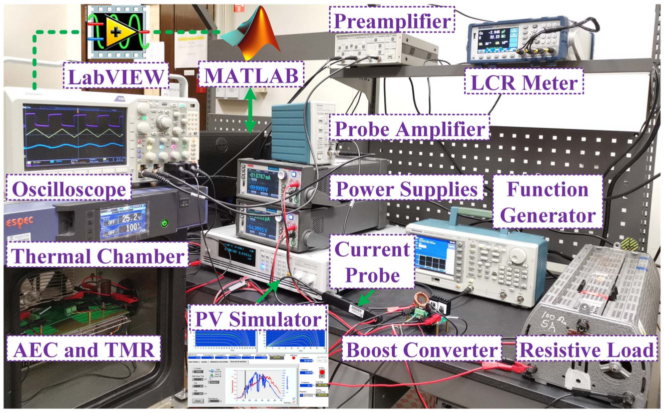

Fig. 7. The experimental setup of the online AEC-monitoring system.

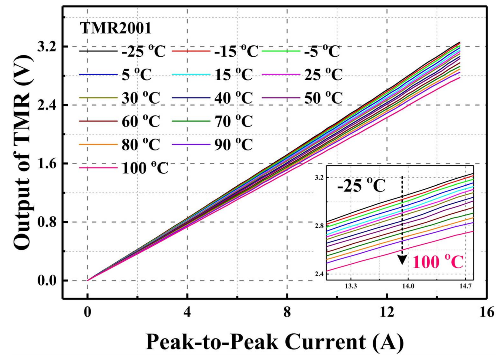

Fig. 8. The output of TMR2001 in the measurement of current up to 15 A from -25 to 100 °C.

TABLE VIII
THE SPECIFICATIONS OF POTENTIAL SENSORS IN AEC MONITORING

Sensor	Manufacturer	Bandwidth (MHz)	Size (cm)	Cost (USD)
Hall-effect current transducer	HY 5-P [38]	0.05	3.6×2.3×1	~21.79
GMR	AA002-02 [39]	1	0.62×0.5×0.4	~9.60
TMR	TMR2001 [34]	1	0.145×0.305×0.3	~1.09
TMR	TMR2901 [40]	1	0.155×0.6×0.49	~44.87

IV. EXPERIMENTAL VALIDATION AND DISCUSSION

The proposed methodologies were validated by the experimental results with the PV simulator. The boost converter with the TMR sensors was integrated on the PCB. The TMR sensors were pre-calibrated. The proposed method was verified in different irradiance and temperature levels. The thermal chamber was used to study the performance of the proposed technique in AEC-monitoring at different temperatures.

A. Experimental Setup

The experimental setup of the online AEC-monitoring system is shown in Fig. 7. It consists of a PV simulator, power supplies, a function generator, a boost converter, voltage probes, a resistive load, a preamplifier, an oscilloscope, a thermal chamber, and a computer. The PV simulator (62020H-150S, Chroma) emulated the PV system in different irradiance and temperature levels. The voltages of AECs were measured by voltage probes. Two TMR2001 were used to measure the magnetic field of the current of input and output AECs for estimations of their ESRs and Cs. The preamplifier (SR560, Stanford Research Systems) was utilized to amplify the output voltages of TMR sensors. The thermal chamber assisted the investigations of AECs at different temperatures. The current and voltage of AECs were obtained from the oscilloscope to the computer through the LabVIEW. The MATLAB was used to analyze the voltage and current to achieve the estimations of ESRs and Cs.

B. Pre-Calibration of TMR sensors

The specifications of the TMR2001 and other potential sensors are summarized in Table VIII. Although the Hall-effect current transducer or giant magnetoresistance (GMR) sensors may be able to be implemented in AEC monitoring, the size of the Hall-effect current transducer is relatively large with higher expense as shown in Table VIII. Furthermore, the Hall-effect current transducer is limited in bandwidth which constrains its application in measuring high-frequency current in power electronic circuits. Generally, the sensitivity of GMR is lower than TMR2001. For example, the GMR AA002-02 with the sensitivity of 4.2 mV/V/Oe is lower than the TMR2001 of 8 mV/V/Oe. Besides, the cost of AA002-02 is higher. Though the TMR2901 has even higher sensitivity of 25 mV/V/Oe, the price is highest as presented in Table VIII. Therefore, the compact and low-cost TMR2001 is chosen and it can be widely implemented in measuring high-frequency current up to 1 MHz in power electronic circuits.

The TMR2001 was soldered on top of the PCB (1.6 mm) of the boost converter and the current wires of AECs were on the bottom of the PCB and right below the TMR2001. Since the TMR2001 was high in sensitivity, it was capable of measuring the current at a distance of 1.6 mm. The bipolar power supply (Kikusui, PBZ 40-10) was used to supply the peak-to-peak current up to 15 A in 20 kHz for the calibration of TMR sensors. The TMR2001 used for input AEC (TMR_IN) and output AEC (TMR_OUT) were pre-calibrated with the current probe (TCPA300, Tektronix). The gain of the preamplifier was fixed at 10 for the TMR sensors. Since the temperature affects the output of TMR sensors, the thermal chamber was utilized to pre-calibrate the TMR2001 at different temperatures. The outputs of TMR2001 in sensing the peak-to-peak current up to 15 A of 20 kHz at the temperature from -25 to 100 °C is shown in Fig. 8. It can be seen that the output peak-to-peak voltage of TMR2001 was in high linearity and decreased with the temperature because the sensitivity of a TMR sensor decreases with temperature [41]. The current for pre-calibration of TMR2001 was increased from 0 to 15 A and then decreased to 0 A. The output of TMR2001 was almost the same for the increasing and decreasing current as Fig. 9 depicts at 25 °C. The polynomial equation can be used to obtain the magnitude of the current sensed by TMR2001 as expressed in Eq. (8).

$$I_{Cal} = a_1 \cdot (T_{avg} - T_o) + b_1 \cdot (T - T_{avg}) + c_1 \cdot T^2 + d_1 \quad (8)$$

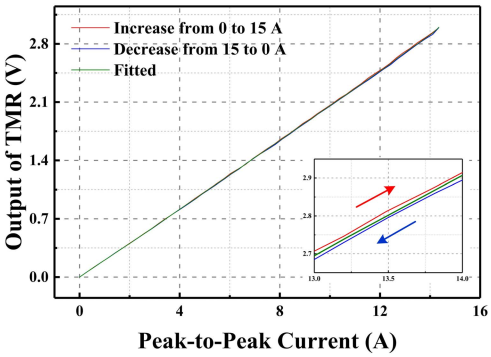

Fig. 9. The output of TMR2001 in the measurement of current increases from 0 to 15 A and then decreases from 15 to 0 A at 25 °C.

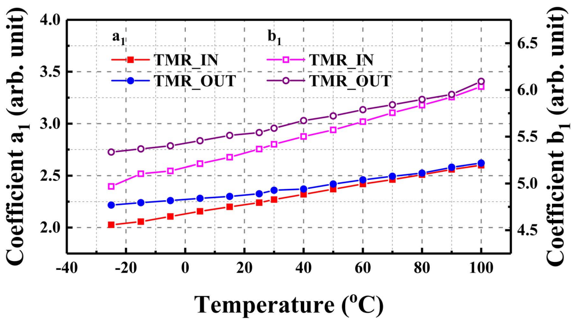

Fig. 10. The fitting results of coefficients a_1 and b_1 from -25 to 100 °C.

where I_{Cal} is the calibrated current, a_1, b_1, c_1, and d_1 depend on the features of TMR2001, T_{avg} is the averaged output, T_o is the offset, and T is the output of TMR2001.

It was proved that the current measured by TMR2001 can be obtained accurately from Eq. (8). The error was within 1.5 % when the current was lower than 0.57 A and within 0.9 % when the current was between 0.57 to 15 A at the temperature from -25 to 100 °C. It is similar to the error (1 %) of commercial Hall-effect current transducer [38]. However, the bandwidth of the Hall-effect transducer is 50 kHz which is much lower than that (1 MHz) of the TMR2001. Furthermore, the compact TMR2001 is even smaller in size (1.45 × 3.05 × 3.0 mm) than the Hall-effect transducer is 12 × 23 × 36 mm. Therefore, the TMR2001 can be integrated on the PCBs of power electronic systems for current measurement.

Since the variations of fitting results of c_1 and d_1 were small from -25 to 100 °C, the averaged c_1 and d_1 can be adopted. The averaged c_1 and d_1 were -0.04885 and -0.02348 respectively for the TMR_IN. For the TMR_OUT, the averaged c_1 and d_1 were -0.05305 and -0.00731. The fitting results of a_1 and b_1 of the TMR_IN and TMR_OUT increased with the temperature from -25 to 100 °C as shown in Fig. 10. This is consistent with the fact that the sensitivity of a TMR sensor decreases with temperature. The errors of the current calculated by Eq. (8) using the averaged c_1 at -25, 25, and 100 °C are shown in Fig. 11 (a), (b), and (c) respectively. The errors were within 2 % for the current less than 0.57 A and within 1.2 % for the current from 0.57 to 15 A. There were phase delays of the current sensed by the TMR sensors which were 58.28° (TMR_IN) and 56.92° (TMR_OUT) from -25 to 100 °C. The phase delays can be compensated digitally

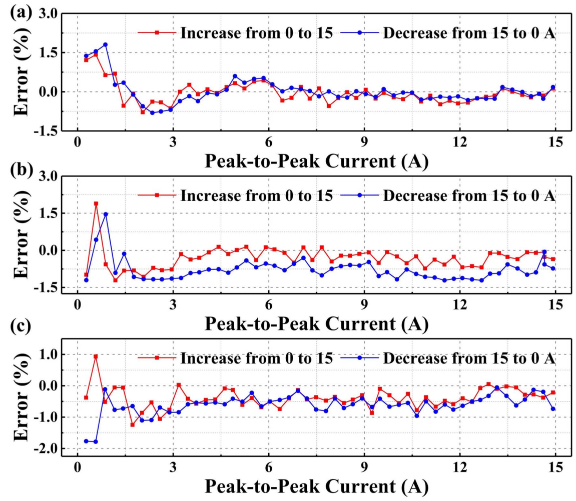

Fig. 11. The accuracy of TMR2001 at (a) -25, (b) 25, and (c) 100 °C.

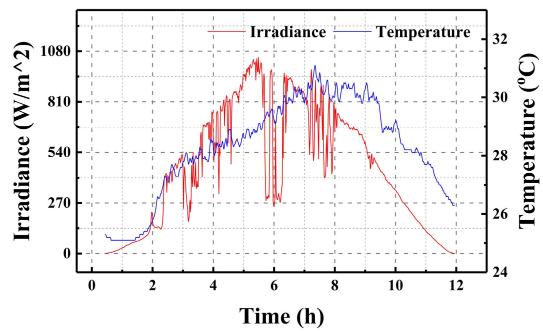

Fig. 12. The irradiance and temperature levels of 12 hours in Hong Kong.

by MATLAB. In summary, the current can be sensed by the TMR2001 accurately and the temperature effects on the TMR2001 can be modeled by Eq. (8).

C. Experiments in Different Irradiance and Temperature Levels and a Variable Load

The irradiance and temperature levels of 12 hours of Hong Kong (22.4°, 114.2°) is shown in Fig. 12. They were imported to the PV simulator to emulate the energy generations of PV systems. The AECs were in the thermal chamber with a constant temperature of 25 °C since the variations of temperature in the 12 hours were insignificant as shown in Fig. 12. The simulation results with the input capacitor of 680 μF and the output capacitor of 1500 μF in the irradiance and temperature levels at 2 h are shown in Fig. 13. The switching noises of the voltage and current were filtered by a digital filter on MATLAB. The current measured by TMR2001 were calibrated by using Eq. (8). The I_{Co} was obtained from the I_L for estimations of ESRs and Cs since the ΔI_{Co} equals the peak of I_L as explained in Section II. B.

The fundamental components of the voltage and current ripples of input and output AECs were acquired from the bandpass filter on MATLAB as Fig. 14 depicts. In this case, the I_{Ci_f} was leading the V_{pv_f} by an angle of 9.13° and the

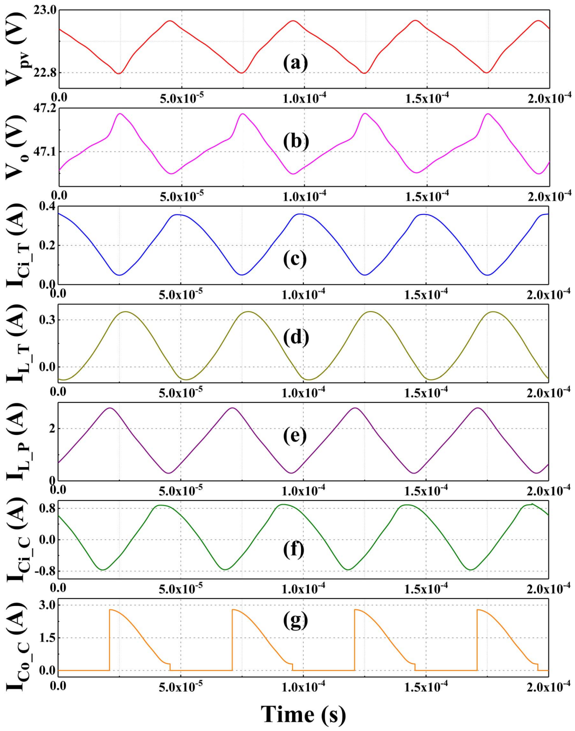

Fig. 13. The voltage and current waveforms with the irradiance and temperature levels at 2 h. (a) the input voltage V_{pv}, (b) the output voltage V_o, (c) the current of input capacitor measured by TMR2001 (I_{Ci_T}), (d) the inductor current measured by TMR2001 (I_{L_T}), (e) the inductor current measured by current probe (I_{L_P}), (f) the calibrated current of input capacitor (I_{Ci_C}), (g) the calibrated current of output capacitor (I_{Co_C}).

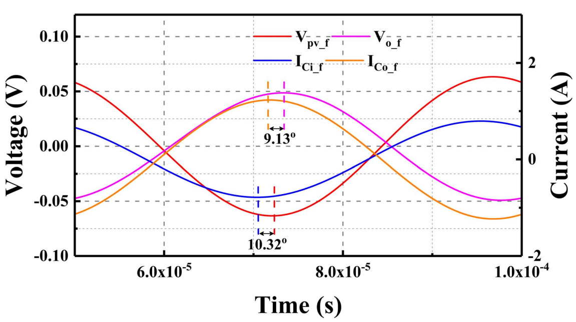

Fig. 14. The fundamental components of the input and output voltage and current.

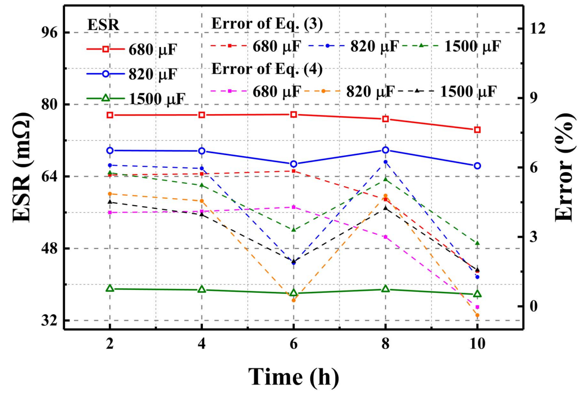

Fig. 15. The estimated ESRs and their errors of the capacitors of 680, 820, and 1500 μF.

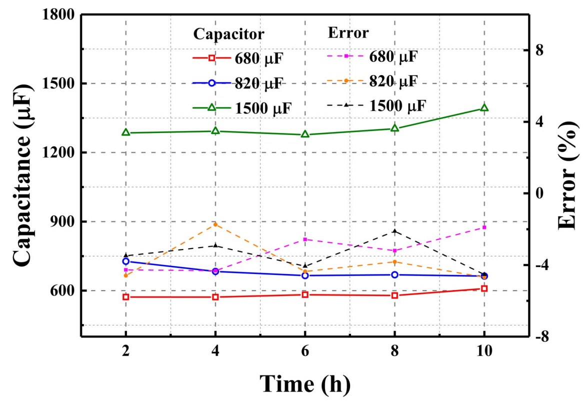

Fig. 16. The estimated Cs and their errors of the capacitors of 680, 820, and 1500 μF.

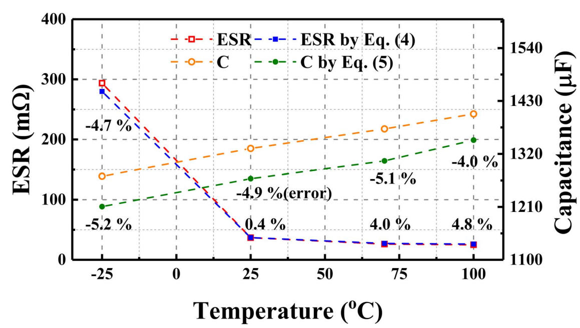

Fig. 17. The estimated ESRs and Cs of the output capacitor from -25 to 100 °C.

I_{Co_f} was leading the V_{o_f} by 10.32°. The estimated ESRs at 2 h are presented in Fig. 15. It can be seen that the proposed method of using Eq. (4) can improve the accuracy from about 6 % to be around 4 %. The experiments with the input capacitor of 820 μF were also conducted. The estimated ESRs and Cs in the irradiance and temperature levels from 2 to 10 h are summarized in Fig. 15 and 16. It was evidenced that the proposed technique could significantly improve the accuracy of ESR-estimations with the error to be within 4.9 %. The proposed method was capable of estimating the C by considering the voltage drops on the C of an AEC. The error was within 4.7 %. Furthermore, it was applicable to PV systems in different irradiance and temperature levels.

The temperature in different places varies greatly. Therefore, it is necessary to evaluate the competence of the proposed technique at different temperatures. A constant irradiance of 500 W/m^2 and temperature of 25 °C was applied to the PV simulator. The temperature of the thermal chamber was varied from -25 to 100 °C and the output AEC was examined. The TMR sensors were calibrated by Eq. (8) with the coefficients at each temperature accordingly. The experimental results of the capacitor of 1500 μF are shown in Fig. 17. The proposed method of Eq. (4) could achieve ESR-estimations with the error of less than 4.8 % from -25 to 100 °C. The proposed

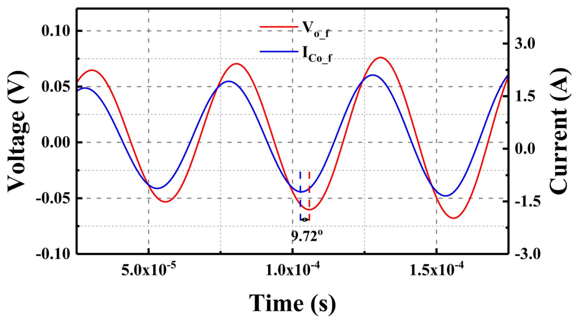

Fig. 18. The fundamental components of the output voltage and current in the transient period when the load varied from 30 to 15 Ω.

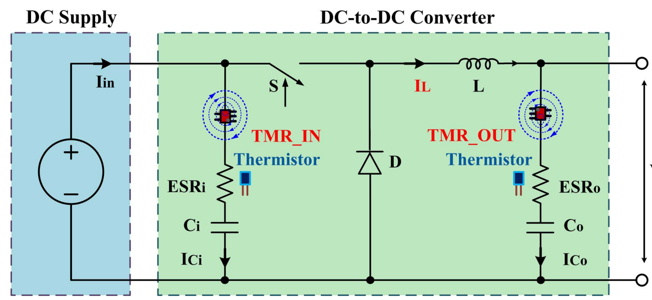

Fig. 19. The AEC monitoring scheme in commercial application with a buck converter.

method of Eq. (5) could achieve the estimation of Cs with the error within 5.2 % from -25 to 100 °C. Hence, it can be concluded that the proposed technique of using magnetoresistive sensors (TMR2001) was competent for the estimations of ESR and C of an AEC in PV systems from -25 to 100 °C.

Although the proposed method of considering the voltage drops on C can estimate the Cs of AECs in high accuracy, the estimated values of Cs are lower than the actual values as shown in Fig. 17 because there is also voltage drops on ESL and it is in the opposite direction of the voltage drops on C in the phasor diagram. According to Eq. (1) and Fig. 1, the voltage drops on ESL are negligible when the frequency is low. Nevertheless, the voltage drops on ESL increase with the operating frequency. Therefore, the estimated values of Cs are lower than the actual values. The errors of estimated Cs will be large when it reaches the resonant frequency of an AEC. However, the accuracy of the estimated ESR will not be affected by the frequency. Hence, a precise health monitoring of AECs can still be achieved.

The performance of the proposed method in the load transient conditions was investigated with a variable load. Similarly, the constant irradiance of 500 W/m^2 and temperature of 25 °C was applied to the PV simulator. The output AEC was tested in the thermal chamber at 25 °C. The load was varied from 30 to 15 Ω. The fundamental components of the output voltage and current are shown in Fig. 18. Since the load resistance decreased, the fundamental components of the output voltage and current ripples increased as shown in Fig. 18. The current was leading the voltage by an angle of 9.72°. The error of the estimated ESR by using Eq. (4) was 4.1 %. The proposed method of Eq. (5) could achieve the estimation of C with an error of 5.4%. Therefore, it can be summarized that the proposed technique was able to estimate the ESR and C accurately in the load transient conditions.

D. Implementation in Commerical Applications

The AECs are widely deployed in energy storage and filtering applications in power electronic systems. The techniques for health monitoring of AEC in commercial applications have been extensively researched since the lifetime of an AEC is limited [42]–[47]. In this paper, the technique using the fundamental components of voltage and current ripples acquired by the TMR sensors are proposed for PV systems. The proposed technique enables predictive maintenance of AECs and contributes to the efficient and reliable operations of PV systems.

The proposed method is also feasible for implementations in other commercial applications. For instance, it can achieve the health monitoring of AECs in a power electronic system with a buck converter as Fig. 19 depicts. Similarly, the MR sensors can be placed nearby the AECs to attain the current. A voltage probe can be used to measure the voltage which is also required for control purposes in power electronic systems. Thus, it does not incur an extra cost. The voltage and current can be analyzed by analog circuits or a software (e.g. MATLAB) to estimate the ESRs and Cs simultaneously. The thermistors can be applied to acquire the temperatures of AECs. Therefore, an online monitoring system based on the proposed technique can be developed by using low-cost and compact MR sensors for commercial applications.

V. Conclusion

The online-monitoring scheme for AECs in PV systems were developed with TMR sensors non-invasively. The temperature effects on AECs and sensors were investigated and modeled effectively from -25 to 100 °C. The simulation and experimental results verified that the proposed methodologies were able to estimate the ESRs with improved accuracy, and the precise estimations of Cs can be achieved by considering the voltage drops on C. It was proved that the cost-effective and compact TMR2001 can be implemented to monitor AECs by estimating ESRs and Cs from -25 to 100 °C. The online-monitoring scheme could realize the AEC-monitoring in PV systems despite the variation of irradiance and temperature levels and load conditions. A promising online-monitoring system of AECs can be developed for a power electronic converter in PV systems and other power systems by the proposed technique.

References

[1] *Renewable Capacity Statistics*, IRENA, Abu Dhabi, United Arab Emirates, 2019.

[2] D. S. Pillai and N. Rajasekar, "A comprehensive review on protection challenges and fault diagnosis in PV systems," *Renew. Sustain. Energy Rev.*, vol. 91, pp. 18–40, Aug. 2018.

[3] H. Wang and F. Blaabjerg, "Reliability of capacitors for DC-link applications in power electronic converters—An overview," *IEEE Trans. Ind. Appl.*, vol. 50, no. 5, pp. 3569–3578, Sep./Oct. 2014.

[4] N. Agarwal, M. W. Ahmad, and S. Anand, "Quasi-online technique for health monitoring of capacitor in single-phase solar inverter," *IEEE Trans. Power Electron.*, vol. 33, no. 6, pp. 5283–5291, Jun. 2018.

[5] M. W. Ahmad, N. Agarwal, P. N. Kumar, and S. Anand, "Low-frequency impedance monitoring and corresponding failure criteria for aluminum electrolytic capacitors," *IEEE Trans. Ind. Electron.*, vol. 64, no. 7, pp. 5657–5666, Jul. 2017.

[6] E. Wolfgang, "Examples for failures in power electronics systems," in *Proc. ECPE Tutorial Rel. Power Electron. Syst.*, Nuremberg, Germany, 2007, pp. 19–20.

[7] Y. Song and B. Wang, "Survey on reliability of power electronic systems," *IEEE Trans. Power Electron.*, vol. 28, no. 1, pp. 591–604, Jan. 2013.

[8] N. Agarwal, A. Arya, M. W. Ahmad, and S. Anand, "Lifetime monitoring of electrolytic capacitor to maximize earnings from grid-feeding PV system," *IEEE Trans. Ind. Electron.*, vol. 63, no. 11, pp. 7049–7058, Nov. 2016.

[9] Y. Gupta, M. W. Ahmad, S. Narale, and S. Anand, "Health estimation of individual capacitors in a bank with reduced sensor requirements," *IEEE Trans. Ind. Electron.*, vol. 66, no. 9, pp. 7250–7259, Sep. 2019.

[10] H. Soliman, H. Wang, and F. Blaabjerg, "A review of the condition monitoring of capacitors in power electronic converters," *IEEE Trans. Ind. Appl.*, vol. 52, no. 6, pp. 4976–4989, Nov./Dec. 2016.

[11] A. M. R. Amaral and A. J. M. Cardoso, "An economic offline technique for estimating the equivalent circuit of aluminum electrolytic capacitors," *IEEE Trans. Instrum. Meas.*, vol. 57, no. 12, pp. 2697–2710, Dec. 2008.

[12] A. M. R. Amaral and A. M. Cardoso, "A simple offline technique for evaluating the condition of aluminum–electrolytic–capacitors," *IEEE Trans. Ind. Electron.*, vol. 56, no. 8, pp. 3230–3237, Aug. 2009.

[13] A. M. Amaral and A. J. M. Cardoso, "Simple experimental techniques to characterize capacitors in a wide range of frequencies and temperatures," *IEEE Trans. Instrum. Meas.*, vol. 59, no. 5, pp. 1258–1267, May 2010.

[14] A. G. Abo-Khalil and D. C. Lee, "DC-Link capacitance estimation in AC/DC/AC PWM converters using voltage injection," *IEEE Trans. Ind. Appl.*, vol. 44, no. 5, pp. 1631–1637, Sep. 2008.

[15] T. H. Nguyen and D.-C. Lee, "Deterioration monitoring of DC-link capacitors in AC machine drives by current injection," *IEEE Trans. Power Electron.*, vol. 30, no. 3, pp. 1126–1130, Mar. 2015.

[16] K. Hasegawa, I. Omura, and S.-I. Nishizawa, "Design and analysis of a new evaluation circuit for capacitors used in a high-power three-phase inverter," *IEEE Trans. Ind. Electron.*, vol. 63, no. 5, pp. 2679–2687, May 2016.

[17] Y. Wu and X. Du, "A VEN condition monitoring method of DC-link capacitors for power converters," *IEEE Trans. Ind. Electron.*, vol. 66, no. 2, pp. 1296–1306, Feb. 2019.

[18] K. Yao, W. Tang, W. Hu, and J. Lyu, "A current-sensorless online ESR and C identification method for output capacitor of buck converter," *IEEE Trans. Power Electron.*, vol. 30, no. 12, pp. 6993–7005, Dec. 2015.

[19] K. Yao, W. Tang, X. Bi, and J. Lyu, "An online monitoring scheme of DC-link capacitor's ESR and C for a boost PFC converter," *IEEE Trans. Power Electron.*, vol. 31, no. 8, pp. 5944–5951, Aug. 2016.

[20] K. Yao, C. Cao, and S. Yang, "Noninvasive online condition monitoring of output capacitor's ESR and C for a flyback converter," *IEEE Trans. Instrum. Meas.*, vol. 66, no. 12, pp. 3190–3199, Dec. 2017.

[21] K. Yao *et al.*, "A noninvasive online monitoring method of output capacitor's C and ESR for DCM flyback converter," *IEEE Trans. Power Electron.*, vol. 34, no. 6, pp. 5748–5763, 2019.

[22] K. Harada, A. Katsuki, and M. Fujiwara, "Use of ESR for deterioration diagnosis of electrolytic capacitor," *IEEE Trans. Power Electron.*, vol. 8, no. 4, pp. 355–361, Oct. 1993.

[23] A. Lahyani, P. Venet, G. Grellet, and P.-J. Viverge, "Failure prediction of electrolytic capacitors during operation of a switchmode power supply," *IEEE Trans. Power Electron.*, vol. 13, no. 6, pp. 1199–1207, Nov. 1998.

[24] P. Venet, F. Perisse, M. H. El-Husseini, and G. Rojat, "Realization of a smart electrolytic capacitor circuit," *IEEE Ind. Appl. Mag.*, vol. 8, no. 1, pp. 16–20, Jan. 2002.

[25] Y.-M. Chen, H.-C. Wu, M.-W. Chou, and K.-Y. Lee, "Online failure prediction of the electrolytic capacitor for LC filter of switching-mode power converters," *IEEE Trans. Ind. Electron.*, vol. 55, no. 1, pp. 400–406, Jan. 2008.

[26] M. A. Vogelsberger, T. Wiesinger, and H. Ertl, "Life-cycle monitoring and voltage-managing unit for DC-link electrolytic capacitors in PWM converters," *IEEE Trans. Power Electron.*, vol. 26, no. 2, pp. 493–503, Feb. 2011.

[27] X.-S. Pu, T. H. Nguyen, D.-C. Lee, K.-B. Lee, and J.-M. Kim, "Fault diagnosis of DC-link capacitors in three-phase AC/DC PWM converters by online estimation of equivalent series resistance," *IEEE Trans. Ind. Electron.*, vol. 60, no. 9, pp. 4118–4127, Sep. 2013.

[28] L. Ren, C. Gong, and Y. Zhao, "An online ESR estimation method for output capacitor of boost converter," *IEEE Trans. Power Electron.*, vol. 34, no. 10, pp. 10153–10165, Oct. 2019.

[29] A. M. Imam, D. M. Divan, R. G. Harley, and T. G. Habetler, "Real-time condition monitoring of the electrolytic capacitors for power electronics applications," in *Proc. 32nd Annu. IEEE Appl. Power Electron. Conf. Expo.*, Anaheim, CA, USA, Feb./Mar. 2007, pp. 1057–1061.

[30] M. W. Ahmad, N. Agarwal, and S. Anand, "Online monitoring technique for aluminum electrolytic capacitor in solar PV-based DC system," *IEEE Trans. Ind. Electron.*, vol. 63, no. 11, pp. 7059–7066, Nov. 2016.

[31] A. Patel and M. Ferdowsi, "Current sensing for automotive electronics-A survey," *IEEE Trans. Veh. Technol.*, vol. 58, no. 8, pp. 4108–4119, Aug. 2009.

[32] J. Lenz and A. S. Edelstein, "Magnetic sensors and their applications," *IEEE Sensors J.*, vol. 6, no. 3, pp. 631–649, Jun. 2006.

[33] W. Miao, X. Liu, K. Lam, and P. W. Pong, "Arc-faults detection in PV systems by measuring pink noise with magnetic sensors," *IEEE Trans. Magn.*, vol. 55, no. 7, Jul. 2019, Art. no. 4002506.

[34] MultiDimension. *TMR2001*. Accessed: Sep. 16, 2019. [Online]. Available: http://www.dowaytech.com/en/index.php?c=download&id=2025

[35] M. L. Gasperi, "Life prediction model for aluminum electrolytic capacitors," in *Proc. IEEE Ind. Appl. Conf. 31st IAS Annu. Meeting*, San Diego, CA, USA, vol. 3, Oct. 1996, pp. 1347–1351.

[36] P. Ingenhoven, G. Belluardo, and D. Moser, "Comparison of statistical and deterministic smoothing methods to reduce the uncertainty of performance loss rate estimates," *IEEE J. Photovolt.*, vol. 8, no. 1, pp. 224–232, Jan. 2018.

[37] N. Kumar, I. Hussain, B. Singh, and B. K. Panigrahi, "Framework of maximum power extraction from solar PV panel using self predictive perturb and observe algorithm," *IEEE Trans. Sustain. Energy*, vol. 9, no. 2, pp. 895–903, Apr. 2018.

[38] LEM. *HY 5-P*. Accessed: Sep. 16, 2019. [Online]. Available: https://docs-apac.rs-online.com/webdocs/12ab/0900766b812ab123.pdf

[39] NVE Corporation. *AA002-02*. Accessed: Sep. 16, 2019. [Online]. Available: https://www.km-cs.com/dir/nve/aa002.pdf

[40] MultiDimension. *TMR2901*. Accessed: Sep. 16, 2019. [Online]. Available: http://www.dowaytech.com/en/1876.html

[41] X. Liu, P. W. T. Pong, and C. Liu, "Dual measurement of current and temperature using a single tunneling magnetoresistive sensor," in *Proc. IEEE Sensors*, New Delhi, India, Oct. 2018, pp. 1–4.

[42] R. Cousseau, N. Patin, C. Forgez, E. Monmasson, and L. Idkhajine, "Improved electrical model of aluminum electrolytic capacitor with anomalous diffusion for health monitoring," *Math. and Comput. Simul.*, vol. 131, pp. 268–282, Jan. 2017.

[43] C. Bhargava, V. K. Banga, and Y. Singh, "An intelligent prognostic model for electrolytic capacitors health monitoring: A design of experiments approach," *Adv. Mech. Eng.*, vol. 10, no. 10, Oct. 2018, Art. no. 1687814018781170.

[44] C. Bhargava, V. K. Banga, and Y. Singh, "Condition monitoring of aluminium electrolytic capacitors using accelerated life testing: A comparison," *Int. J. Qual. Rel. Manage.*, vol. 35, no. 8, pp. 1671–1682, Sep. 2018.

[45] K. Hasegawa, S. Nishizawa, and I. Omura, "ESR and capacitance monitoring of a dc-link capacitor used in a three-phase PWM inverter with a front-end diode rectifier," *Microelectron. Rel.*, vols. 88–90, pp. 433–437, Sep. 2018.

[46] N. Khera and S. A. Khan, "Prognostics of aluminum electrolytic capacitors using artificial neural network approach," *Microelectron. Rel.*, vol. 81, pp. 328–336, 2018.

[47] N. Khera and S. A. Khan, "Real-time reliability monitoring of DC-link capacitors in back-to-back converters," *Energies*, vol. 12, no. 12, pp. 328–336, Feb. 2019.

Wenchao Miao received the B.Eng. degree in electrical and electronic engineering from the University of Nottingham, U.K. He is currently pursuing the Ph.D. degree with the Department of Electrical and Electronic Engineering, The University of Hong Kong, Hong Kong. His current research interests include the applications of magnetoresistive sensors in power systems, faults detection in DC systems, and the condition monitoring of photovoltaic systems.

K. H. Lam received the bachelor's degree in electrical energy systems engineering and the Ph.D. degree in architecture from The University of Hong Kong, Hong Kong, in 1994 and 2007, respectively. He was with the building services industry after graduation and returned to his Alma Mater, joined the HKU Photovoltaic Research Team, in 1998. He started to work as a Senior Manager with Solar Energy Company. From 2008 to 2009, he was the Chairman of the Hong Kong Photovoltaic Consortium. In 2014, he was appointed as a Lecturer with the Department of Electrical and Electronic Engineering, The University of Hong Kong, where he became an Honorary Assistant Professor in 2016. He is a Lecturer with The University of Hong Kong. His current research interest includes photovoltaic systems integration. He is also a Registered Chartered Electrical Engineer with the Engineering Council, U.K., and a Registered Energy Assessor with the Hong Kong Government.

Philip W. T. Pong (SM'13) received the Ph.D. degree in engineering from the University of Cambridge in 2005. After working as a Post-Doctoral Researcher with the Magnetic Materials Group, National Institute of Standards and Technology (NIST), USA, for three years, he joined the Department of Electrical and Electronic Engineering (EEE), The University of Hong Kong (HKU), Hong Kong, where he is currently a tenured Associate Professor working on development and the applications of magnetoresistive sensors and contactless sensing technologies in smart grid and smart living. He has published more than 120 SCI journal papers with around 1700 citations. His current research interests include magnetoresistive sensors and smart grid. He is a fellow of the Institution of Engineering and Technology (FIET), the Institute of Materials, Minerals and Mining (FIMMM), the Energy Institute (FEI), and the NANOSMAT Society (FNS). He is a Corporate Member of HKIE in electrical, electronics, and energy divisions. He serves on the Editorial Board for two SCI journals and on the Editorial Review Board of the IEEE MAGNETICS LETTERS. He is also a Chartered Physicist, a Chartered Electrical Engineer, and a Chartered Energy Engineer. He is a Registered Professional Engineer of Electrical, Electronics, and Energy in Hong Kong. From 2019 to 2022, he was the ACM Distinguished Speaker on the topic of contactless sensing and smart living.